

Enhanced recovery of phosphate and ammonium from aqueous solution by wheat straw biochar modified by oyster shell

Peng Dong, Jing Yu, Liang Chen, Guibin Pang*

School of Water Conservancy and Environment, University of Jinan, Jinan 250022, China, emails: stu_panggb@ujn.edu.cn (G. Pang), dongpeng199708@163.com (P. Dong), yz0101j@163.com (J. Yu), chenliang202129@163.com (L. Chen)

Received 26 April 2023; Accepted 24 August 2023

ABSTRACT

In this study, the effect of oyster shell powder as a substitute for calcium chemical reagents to modify straw biochar for enhancing removal of phosphate and ammonium from aqueous solution was investigated. The results showed that the biochar composite (OSB3:1) with the maximum capacity (151.37 mg-P/g and 0.8 mg-N/g) was synthesized at optimum mass ratio of oyster shell-to-straw (3:1) and pyrolysis temperature (800°C). The adsorption process followed the Langmuir isotherm and pseudo-second-order kinetic models, and it achieved excellent performance at pH 2.0–11.0. According to the thermodynamic analysis, the adsorption reaction was an endothermic and spontaneous process, and increasing the temperature increased the adsorption capacity. The removal mechanisms for phosphate included the formation of hydroxyapatite precipitation, ligand exchange, surface complexation and electrostatic attraction, while for ammonium only electrostatic attraction. The modified biochar can effectively remove phosphate (over 85%) from real domestic sewage within 3 h. Reuse of P-laden biochar as heavy metal adsorbent was proposed, as it exhibited a good removal efficiency for Cd, Zn and Cu, especially application for acidic wastewater.

Keywords: Biochar; Oyster shell; Phosphate; Adsorption; Ammonium; Co-pyrolysis

1. Introduction

Phosphorus (P) and nitrogen (N) are extremely important elements in maintaining the growth and development of organisms [1]. The excessive discharge of P and N into environment will cause negative impact on the ecosystem, such as eutrophication, water quality deterioration, and ecological degradation [2]. Therefore, a series of strict discharge standards (0.5 mg/L in China) had been enacted and implemented in many countries. In the meanwhile, the natural reserves of P will be depleted within the next 100 y, at the current rate of human use [3]. In recent years, the recycling of excess phosphate and ammonium from water has attracted intensive attention to solve eutrophication in water body and phosphorus recovery.

At present, some methods (e.g., chemical treatment and biological treatment) have been applied in phosphate and ammonium removal from wastewater [4–6]. However, the relatively high cost and low efficiency of some processes have hindered their application in wastewater treatment. In contrast, adsorption has been proven to be an efficient and feasible technology for eutrophication control in water body due to its high selectivity and practicality [7,8].

Many studies showed biochar had a good adsorption capacity on organic pollutants and cations. In contrast, the adsorption capacity of biochar on anionic pollutants such as phosphate was relatively limited [9]. Therefore, it is essential to modify biochar to enhance the adsorption capacity for phosphate. According to previous studies, metal cations

* Corresponding author.

(Mg^{2+} , Ca^{2+} , Al^{3+} , Fe^{3+} , La^{3+} , etc.) modification can effectively enhance the adsorption performance of biochar for phosphate [10,11]. However, many metal ions (e.g., Al^{3+} , Fe^{3+} , La^{3+}) loaded on biochar could be released into the water in the process of adsorption, which will affect the growth of aquatic organisms. Among the cations used for biochar modification, calcium (Ca) is an ideal cation for biochar modification, due to its easy availability, low-cost, and friendliness to ecological environment. Many studies reported that Ca chemical reagents (e.g., $CaCl_2$, $Ca(OH)_2$) modified biochar for effective removal phosphate from water. The adsorption capacity of $CaCl_2$ -modified granular attapulgite was increased by 12 times than that of raw material [12]. Wang et al. [13] prepared calcium-modified flour biochar with the maximum sorption capacity of 314.22 mg/g. Usually, calcium-modified biochar is prepared by loading Ca chemical reagent such as $CaCO_3$, $Ca(OH)_2$, or $CaCl_2$ onto the surface of biochar for modification. In order to reduce the cost, the preparation of modified adsorbents based on Ca-rich waste has received intensive attention. Oyster shell is a common biowaste containing about 95% calcium carbonate, so the modification of biochar with oyster shell as a calcium source substitute could be an attractive approach. Moreover, the post-adsorption (P-laden) modified biochar has the potential to be used as adsorbent to remove heavy metals from aqueous solution, or as a slow-releasing fertilizer for soil.

In this study, oyster shell-modified biochar composites were prepared by the co-pyrolysis of oyster shell (as the calcium source) and wheat straw. The effect of mass ratio of oyster shell-to-straw and pyrolysis temperature was investigated to reveal the optimum ratio and pyrolysis temperature. Adsorption experiments and related models were used to determine the adsorption properties of the synthesized biochar composites on both phosphate and ammonium. The performance of nutrients removal from real domestic sewage by the synthesized material was also investigated. The removal mechanisms on phosphate and ammonium were also examined.

2. Materials and methods

2.1. Materials

Wheat straw samples were collected from a farm and oyster shells were attained from a food market in Jinan City, Shandong Province, China. The samples were washed three times with deionized water and dried in an oven at 105°C for 12 h. The samples were crushed and sieved through 0.1 mm sieve. The phosphate solution used for the following experiments was prepared by diluting the stock solution (500 mg-P/L).

Chemical reagents used in this experiment were all of analytical grade, including ammonium molybdate tetrahydrate ($(NH_4)_6Mo_7O_{24} \cdot 4H_2O$), L-ascorbic acid ($C_6H_8O_6$), potassium dihydrogen phosphate (KH_2PO_4), ammonium chloride (NH_4Cl) which were produced by Sinopharm Chemical Reagent Co., Ltd., (Shanghai, China), antimony potassium tartrate ($C_4H_4KO_5Sb \cdot 0.5H_2O$) produced from Chengdu Jinshan Chemical Reagent Co., Ltd., (Chengdu, China), and Nessler's reagent (for ammonium measurement) produced by Beckman Biotechnology Co., Ltd. (Changde, China).

2.2. Preparation of biochar

The preparation of biochar composites by pyrolysis of material powders in a high-temperature tube furnace (OTF-1200X, Kejing, China). The modified biochar composites were prepared with oyster shell and wheat straw powders at mass ratios of 0:1, 1:1, 2:1, 3:1, 4:1, 5:1, and 1:0, respectively, and the mixture was heated to 800°C for 2 h at a rate of 10°C/min in the presence of nitrogen stream. The chamber was then cooled to room temperature to obtain the modified biochar (OSB). The biochar mixtures with mass ratios of 0:1, 1:1, 2:1, 3:1, 4:1, 5:1 and 1:0 was named biochar (BC), OSB1:1, OSB2:1, OSB3:1, OSB4:1, OSB5:1, OSB.

To investigate the influence of pyrolysis temperature on phosphate adsorption capacity of the modified biochar, the mixture of oyster shell and wheat straw powders at a mass ratio of 3:1 was pyrolyzed at 600°C, 700°C, 800°C, and 900°C and the synthesized materials were named 600OSB, 700OSB, 800OSB (OSB3:1) and 900OSB, respectively.

2.3. Phosphate adsorption experiments

All batch adsorption experiments were performed in plastic bottles. Typically, 0.1 g of the material was put into a 100 mL polyethylene bottle containing 40 mL of phosphorus solutions at room temperature, and filtered with 0.45 μm filter paper after 24 h, and then the concentration of phosphate was determined by ammonium molybdate spectrophotometric method at a wavelength of 700 nm with a UV-Vis Spectrophotometer (T6 New Century, Beijing Persee General Instrument Co., Ltd., China). Adsorption isotherm was investigated with 0.1 g of the prepared materials and 40 mL solutions containing phosphate concentration (0–400 mg-P/L) at pH 7.0. The adsorption kinetic properties were examined by mixing different materials and 100–200 mg-P/L solutions, and samples were collected at specified times (0–1,440 min) for the measurement of phosphate concentration. The influence of pyrolysis temperature of biochar on phosphate adsorption was examined with the addition of 0.1 g of the materials (600OSB, 700OSB, 800OSB, and 900OSB) into 40 mL phosphate solution (100 mg-P/L) for 24 h. Meanwhile, the initial pH of the solution is adjusted to be in the range of 2–11 to study the effect of pH. To study the effect of co-existing anions, 0.1 g of material and 40 mL solution (5 mmol-P/L) with different anions (NO_3^- , HCO_3^- , SO_4^{2-} and Cl^-) with the concentrations of 0–40 mmol/L were mixed for 24 h, and the mixture was immediately filtered, and the concentrations of phosphate were measured.

2.4. Ammonium adsorption experiments on modified materials

Ammonium is a common pollutant in actual domestic wastewater. To study the effect of pH on ammonium adsorption, 0.1 g OSB3:1 and 40 mL ammonium solution (10 mg-N/L) were mixed, and the initial pH of the solution was adjusted to different initial pHs (2, 3, 5, 7, 9, 11) using NaOH and HCl solutions. The adsorption isotherm properties were studied by mixing 0.1 g OSB3:1 and 40 mL ammonium solution varying the initial ammonium concentration (0.5, 1, 2, 5, 8, and 10 mg/L).

2.5. Treatment of real domestic wastewater with modified biochar

The synthetic material (OSB3:1) was used to adsorb phosphate and ammonia from real domestic wastewater from the inlet and outlet of one sewage treatment station University of Jinan, Shandong Province. Three dosage of adsorbents (1.25, 2.5 and 5.0 g/L) of adsorbent were used to remove nutrients from real sewage wastewater, and samples were taken at specified times (0, 5, 10, 20, 30, 60, 120, and 180 min) for were phosphate concentration measurement after being filtered through 0.45 μm filter.

2.6. Application of P-laden biochar as metals adsorbent

The feasibility of reusing P-laden biochar to remove heavy metal ions from aqueous solutions was investigated. 0.05 g P-laden OSB3:1 was placed into 25 mL heavy metal solution (Cu^{2+} , Cd^{2+} and Zn^{2+} (100 mg/L)) at the initial pH 1.5, 2, 3 and 4 for 24 h. After reaction, the filtrate was used for metals concentrations analyzing by using atomic absorption spectroscopy (AAS, AA-7000, Shimadzu, Japan).

2.7. Material characterization

The micro-morphological structure and surface elemental constitute of the samples was characterized by scanning electron microscopy (SEM, Tescan Mira LMS, Czech) equipped with energy-dispersive X-ray spectrometer (EDS). The specific surface area (S_{BET}) and pore size

distribution was measured by Brunauer–Emmett–Teller (BET) analyzer (Micromeritics ASAP 2460, USA). The surface functional groups of the samples were analyzed using Fourier-transform infrared spectroscopy (FTIR) in the range of 400–4,000 cm^{-1} (Thermo Nicolet iS50, USA). The crystal structure of the materials was determined by X-ray powder diffractometry (XRD, Rigaku Ultima IV, Japan).

3. Results and discussion

3.1. Material characterization

The morphology and structure of the synthesized materials (BC, OSB3:1, and P-laden OSB3:1) are shown in Fig. 1. OSB3:1 had a relatively smooth surface with some spherical particles. After adsorption, many flocculent precipitates appeared on the surface of biochar, resulting in a decrease in pore size and loss of active adsorption sites. Compared to OSB3:1, the mass fraction (%) of P increased from 1.4% to 8.5% after adsorption, indicating that P was transferred from the aqueous solution to the adsorbent during the adsorption process.

The XRD spectra of OSB3:1 before and after adsorption are shown in Fig. 2b. The diffraction peaks of CaO ($2\theta = 32.5^\circ, 37.8^\circ, 54.2^\circ, 64.7^\circ, 67.7^\circ, 79.9^\circ,$ and 88.8°) were observed for OSB3:1 [14]. While, after phosphate adsorption, the diffraction peak of CaO disappeared and the new peaks of hydroxyapatite ($\text{Ca}_5(\text{PO}_4)_3\text{OH}$) appeared at $2\theta = 28.8^\circ, 29.5^\circ, 32.1^\circ, 39.4^\circ, 49.5^\circ,$ and $\text{Ca}(\text{OH})_2$ at $2\theta = 18.2^\circ, 34.4^\circ,$

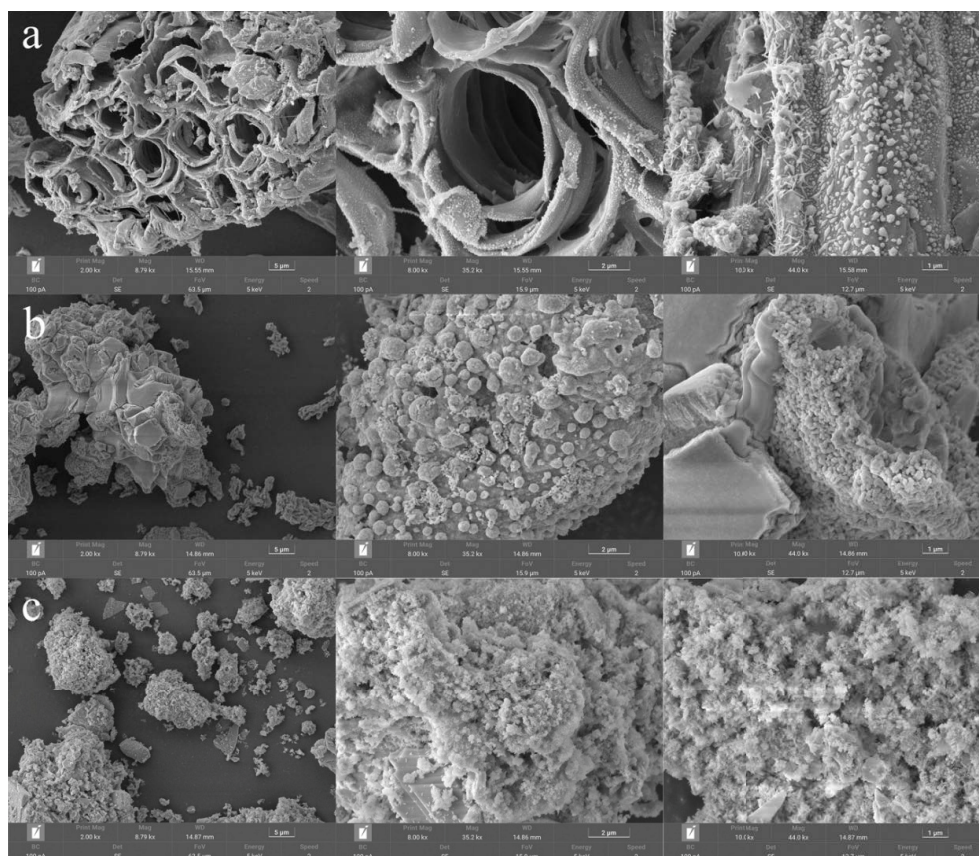


Fig. 1. Scanning electron microscopy images of BC (a), OSB3:1 (b) and P-laden OSB3:1 after adsorption (c).

47.3°, 51.0°, 54.5° [15]. Meanwhile, pyrolysis temperature and mixing ratio (oyster shell and wheat straw) had great impact on the minerals formed in the synthesized materials (Fig. 2a and c). For 600OSB and 700OSB, the main diffraction peaks were attributed to CaCO_3 and no diffraction peaks of CaO were observed in the XRD patterns. While diffraction peaks of CaO were observed in the XRD patterns for 800OSB (OSB3:1). It indicated that pyrolysis temperature no less than 800°C would be required for the preparation of the materials for effective phosphate adsorption [16,17].

Compared with the adsorption capacity (11.06 mg·P/g) and S_{BET} (323.51 m^2/g) of raw straw biochar, OSB3:1 had superior adsorption capacity for phosphate (151.37 mg/g) with very low S_{BET} (3.62 m^2/g). It suggested that the predominant mechanism could be chemical adsorption rather than physical adsorption. The pore volumes and average pore sizes for BC and OSB 3:1 were 0.23 and 0.0063 cm^3/g , 2.85 and 6.77 nm (Table 1), respectively, indicating that the introduction of Ca promoted the formation of pore structure [2,13].

The results of surface functional groups on the synthesized materials are shown in Fig. 3. The band at 3,643 cm^{-1} was attributed to the stretching vibration of $-\text{OH}$, and the bands at 712, 874 and 1,419 cm^{-1} represented the bending vibration of CO_3^{2-} . Compared with the BC, the diffraction peaks of the $-\text{OH}$ and CO_3^{2-} groups of the oyster

Table 1
Basic physical properties of modified biochar

Samples	S_{BET} (m^2/g)	Pore volume (cm^3/g)	Pore size (nm)
800BC	323.51	0.23	2.85
800OSC	1.82	0.0035	7.75
OSB1:1	107.91	0.0672	2.49
OSB2:1	7.19	0.0089	4.93
OSB3:1	3.62	0.0063	6.77
OSB4:1	2.32	0.0034	6.16
OSB5:1	2.53	0.0042	6.70

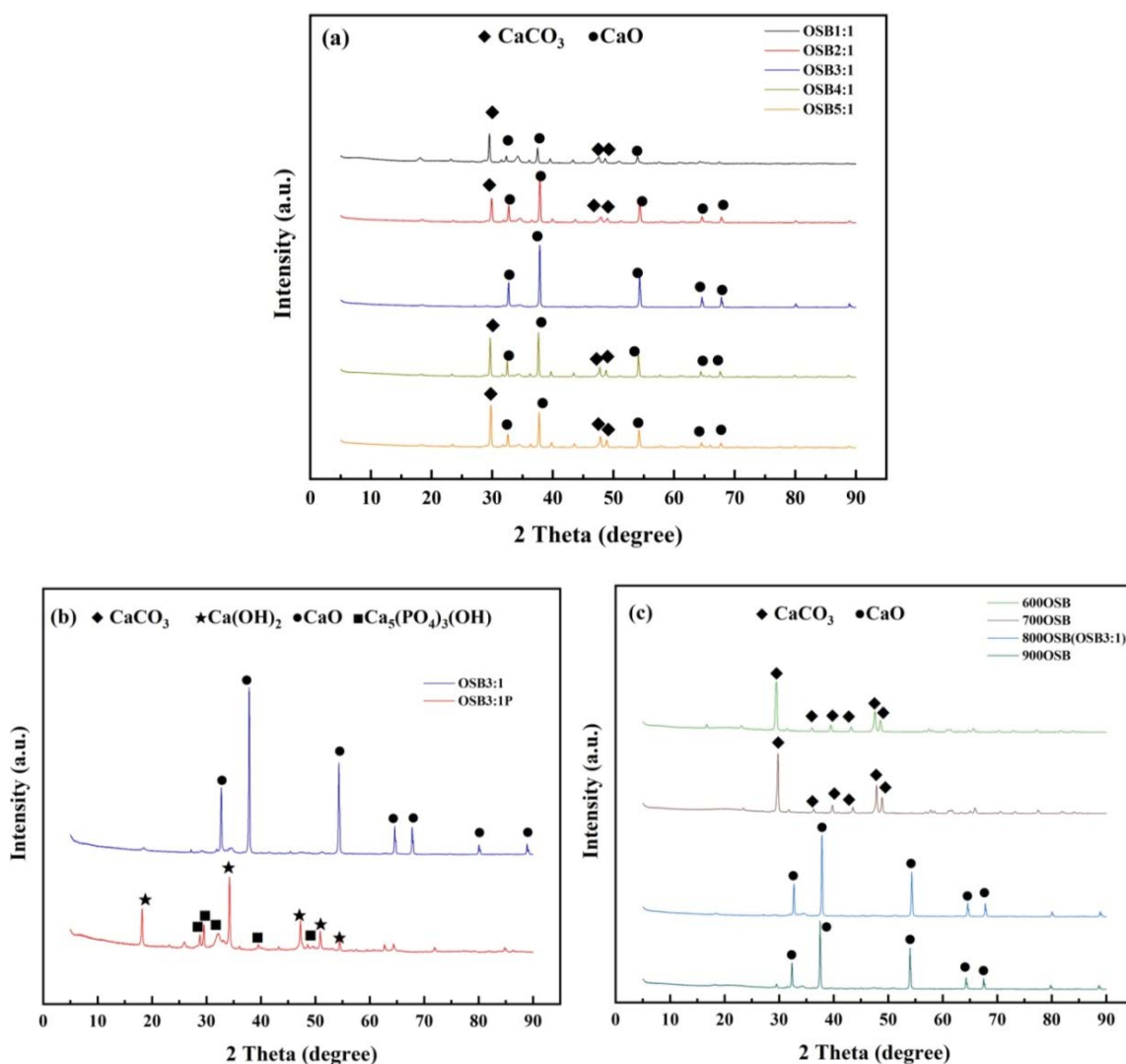


Fig. 2. X-ray diffraction spectra of synthetic materials.

shell modified biochar (OSB3:1) were obviously enhanced because of the modification of the oyster shell. After adsorption, new peaks were observed at 1,050 cm⁻¹, which was attributed to the P=O stretching vibration band.

3.2. Adsorption experiments

3.2.1. Effect of pyrolysis temperature and solution initial pH on adsorption capacity

As shown in Fig. 4a, the biochars pyrolyzed at 800°C and 900°C had higher adsorption capacity than those pyrolyzed at 600°C and 700°C at pH 2–11. For example, the adsorption capacity for 600OSB, 700OSB, 800OSB and 900OSB at pH 2.0–11.0 was 24.48–32.05, 25.87–36.89, 40.58–43.82, and 40.57–43.65 mg·P/g, respectively. At pyrolysis temperatures of 800°C and 900°C, CaCO₃ in oyster shell powder

was decomposed into CaO (Fig. 2c) and it could introduce active Ca(II) into the biochar, which improved the adsorption capacity of biochar for phosphate. It suggested that the pyrolysis temperature (800°C) would be required for preparing oyster shell modified straw biochar with high adsorption efficiency.

The pH of the solution is an important factor in the removal of phosphate from complex materials, as it can affect the species distribution of P in solution and the characteristics of the adsorbent surface. As shown in Fig. 4a. The result indicated that the efficient removal of phosphate can be achieved at wide pH range (2.0–11.0) with the maximum at initial pH 2.0. In addition, the pH of the solution increased after phosphate adsorption, indicating its advantage in the treatment of acidic wastewater containing P (Fig. 4b).

3.2.2. Adsorption kinetics

The pseudo-first-order kinetic model [Eq. (1)], pseudo-second-order kinetic model [Eq. (2)], intraparticle diffusion model [Eq. (3)], and mass transfer factor (MTF) models [Eqs. (4)–(6)] were employed to fit the experimental data to evaluate the adsorption kinetic performance of the modified biochar [19–21].

$$\ln(Q_e - Q_t) = \ln Q_e - k_1 t \tag{1}$$

$$\frac{t}{Q_t} = \frac{1}{k_2 Q_e^2} + \frac{t}{Q_e} \tag{2}$$

$$Q_t = K_t t^{0.5} + C \tag{3}$$

$$\ln\left(\frac{C_0}{C_t}\right) = [k_L a]_g \times e^{-\beta \times q} \times t \tag{4}$$

$$q = \frac{1}{\beta} \times \ln t + B \tag{5}$$

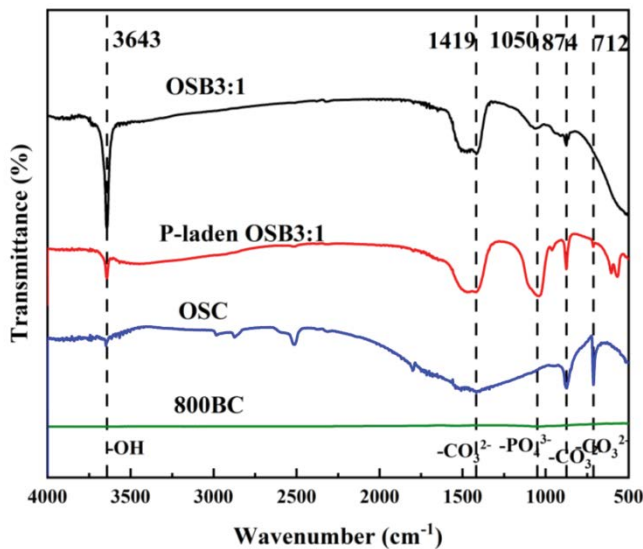


Fig. 3. Fourier-transform infrared spectra of synthetic materials.

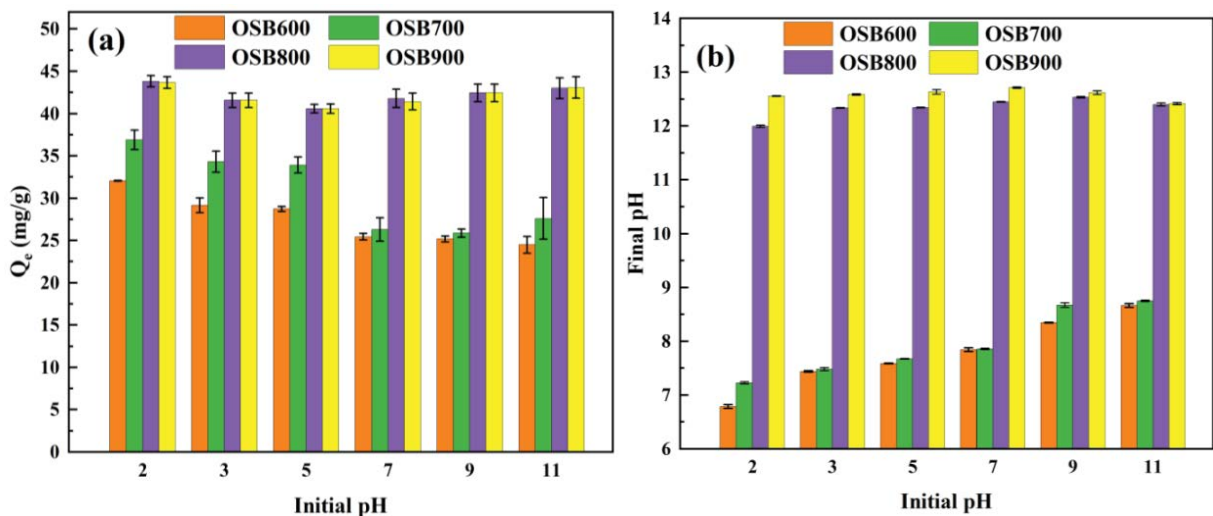


Fig. 4. (a) Effect of initial pH on adsorption capacity of synthetic materials, and (b) final pH after phosphate adsorption.

$$B = \frac{\ln\left(\left[k_L a\right]_g\right) - \ln\left\{\ln\left(\frac{C_0}{C_t}\right)\right\}}{\beta} \quad (6)$$

where Q_e and Q_t (mg/g) are the sorption capacity of the adsorbent at the time of adsorption equilibrium and time t , respectively; k_1 (min^{-1}) and k_2 (g/mg·min) refer to the rate constants of the proposed pseudo-first-order and pseudo-second-order kinetic models, respectively [21]; K_i (mg/g·min^{1/2}) refers to the intraparticle diffusion rate constant, and C is a variable that is dependent on the depth of the adsorption border [12]. C_0 is initial concentration of the phosphate in the solution (mg/L), and C_t is concentration of the phosphate remaining in the solution at a time t (mg/L). $[k_L a]_g$ is global mass transfer factor (min^{-1}), β is adsorbate–adsorbent affinity parameter (g/min·mg), and t is accumulation time (min). B is potential mass transfer index relating to driving force of mass transfer (mg/g) [22].

From Fig. 5a, the adsorption of phosphate onto OSB3:1 increased rapidly within 3 h and reached equilibrium

within 6 h. The pseudo-second-order kinetic model had a higher determined coefficient compared to that of the pseudo-first-order kinetic model (Table 2). According to the pseudo-second-order kinetic model, the theoretical adsorption capacities were 44.31 and 72.70 mg/g when adsorption reached equilibrium at phosphate concentrations of 100 and 200 mg/L, which were closer to the actual adsorption capacities of 42.89 and 65.79 mg/g when equilibrium reached. This suggested that the adsorption of phosphate onto OSB3:1 could be dominated by chemisorption (e.g., complexation, precipitation ligand exchange and other chemical reactions). The adsorption rate constant k_2 of 200 mg/L was higher than that of 100 mg/L, showing that more time was required to reach equilibrium at higher phosphate concentrations. The fitting results of the intraparticle diffusion model showed that the adsorption process was divided into two different stages, with the first stage having a higher slope and the next stage having a lower slope [23]. This can be interpreted that at the first stage phosphate in the solution contact with the outer surface of the OSB3:1 material, and at the second stage phosphate ions enter the pores of

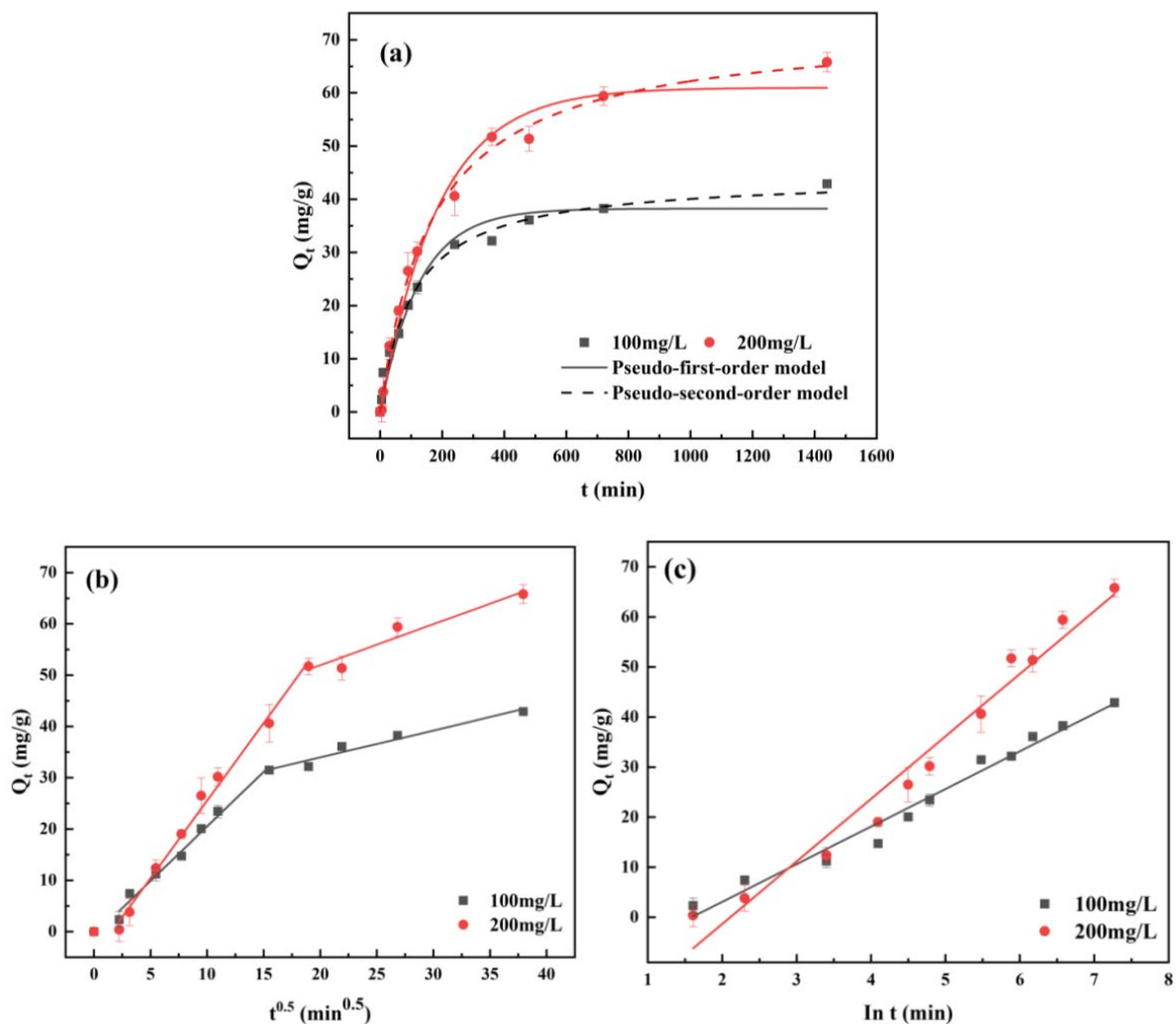


Fig. 5. Adsorption kinetics of phosphate onto OSB3:1, (a) pseudo-first-order kinetics and pseudo-second-order kinetics, (b) internal diffusion model, and (c) mass transfer model.

OSB3:1 and react with Ca²⁺ in the material (Fig. 5b). The fitting result of the MTF model is presented in Fig. 5c and the parameters are presented in Table 2. The fitted line had a smaller slope at lower P concentration, which implies a lower 1/β and a lower binding resistance of the adsorbent to adsorbate [22]. It showed that 1/β increased from 7.52 to 12.49 g·min/mg and B decreased from -11.96 to -26.33 mg/g as C₀ was increased from 100 to 200 mg/L, implying that the rate of the phosphorus adsorption by the modified material increased with the initial P concentration.

3.2.3. Adsorption isotherms

The Langmuir [Eq. (7)] and Freundlich [Eq. (8)] isotherm models were used to fit the data of adsorption [24].

$$Q_e = K_L \cdot Q_{\max} \cdot \frac{C_e}{1 + K_L \cdot C_e} \tag{7}$$

$$Q_e = K_F \cdot C_e^{1/n} \tag{8}$$

where Q_e (mg/g) is the equilibrium sorption capacity, C_e (mg/L) is the equilibrium concentration of the adsorbate, and Q_{max} is the maximum sorption capacity. K_L (L/mg) is the Langmuir adsorption equilibrium constant. K_F ((mg/g) (L/mg)^{1/n}) is the Freundlich isotherm constant related to the adsorption capacity of the adsorbate, and n is a constant related to adsorption intensity. Further, the basic characteristics of Langmuir can be expressed by dimensionless factor R_L according to Eq. (9).

$$R_L = \frac{1}{1 + K_L C_0} \tag{9}$$

where R_L is the dimensionless separation factor, which reflects the favorability of adsorption.

The adsorption isotherm is shown in Fig. 6, and the fitting parameters are summarized in Table 3. The determined

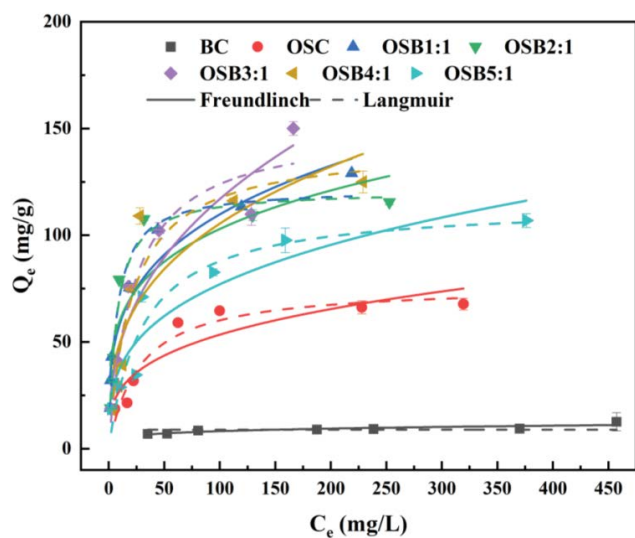


Fig. 6. Adsorption isotherms of synthetic materials.

Table 2
Adsorption kinetic parameters of phosphate on 800OSB material

Phosphorus concentrations (C ₀)	Pseudo-first-order model			Pseudo-second-order model			Intraparticle diffusion model				Mass transfer kinetics				
	k ₁ (min ⁻¹)	Q _e (mg/g)	R ²	k ₂ (g/mg·min)	Q _e (mg/g)	R ²	k ₁ (mg/g·min ^{1/2})	k ₂ (mg/g·min ^{1/2})	C ₁ (mg/g)	C ₂ (mg/g)	R ² ₁	R ² ₂	B (mg/g)	1/β (g/min·mg)	R ²
100 mg/L	0.008	38.24 ± 1.49	0.970	0.000213	44.31 ± 1.33	0.990	2.13	0.8	-0.78	35.95	0.987	0.936	-11.96	7.52	0.976
200 mg/L	0.005	60.97 ± 2.05	0.985	0.000082	72.70 ± 1.60	0.996	3.03	0.52	-4.74	23.46	0.992	0.958	-26.33	12.49	0.970

coefficient (R^2) of the Langmuir model (0.898–0.966) was higher than that of the Freundlich model (0.762–0.952), suggesting the adsorption of phosphate onto the modified biochar was mainly monolayer adsorption. Among the synthesized materials, the adsorption capacity of the raw BC for phosphate was very low (Q_{\max} 11.06 mg-P/g), while its adsorption capacity (Q_{\max}) increased substantially to 151.37 mg-P/g after modification, mainly due to the introduction of Ca^{2+} from oyster shells into the biochar during the modification process. BC (with maximum S_{BET}) had the lowest adsorption capacity, while, the adsorption capacity of phosphate onto Ca^{2+} modified biochar was greatly improved even with low S_{BET} , which indicated that physical adsorption did not play a key role in the adsorption process. The parameter (R_L) is an important metrics for evaluation the isothermal adsorption performance of Langmuir, and R_L values in the range of 0–1 indicated that the adsorption process was favorable (Table 3). In addition, the $1/n$ values for the Freundlich isotherm were all below 1.0, which indicated that the adsorption of phosphate onto the biochar was easy to occur.

Among the modified biochars (pyrolyzed at different temperature and mixing ratio), OSB3:1 (800OSB) had the best removal performance with Q_{\max} 151.37 mg/g,

which was comparable to those reported in the literature (Table 4). It suggested the efficient adsorbent for phosphate was prepared with optimum mixing ratio (3:1) of oyster shell to straw and pyrolyzed at 800°C.

3.2.4. Adsorption thermodynamics

Adsorption experiments were conducted at 277, 298, and 318 K to examine the effect of temperature on phosphate adsorption. Thermodynamic analysis was performed by calculating its thermodynamic parameters using the following equations [Eqs. (10) and (11)].

$$\Delta G^\circ = -RT \ln K_d \quad (10)$$

$$\ln K_d = \frac{\Delta S^\circ}{R} - \frac{\Delta H^\circ}{RT} \quad (11)$$

where K_d is the thermodynamic equilibrium constant; ΔG° (kJ/mol), ΔH° (kJ/mol) and ΔS° (J/mol·K) represent the free energy, enthalpy, and entropy changes, respectively; R (8.314 J/mol·K) is a constant; and T (K) is the thermodynamic temperature [36,37].

Table 3
Fitting parameters of the adsorption isotherm for phosphate on synthetic materials

Absorbents	Freundlich			Langmuir			
	K_f ((mg/g)(L/mg) ^{1/n})	1/n	R^2	K_L (L/mg)	Q_{\max} (mg/g)	RSD	R^2
800BC	3.32	0.20	0.781	0.04	11.06 ± 0.90	8.14%	0.674
OSC	13.88	0.29	0.841	0.04	76.67 ± 5.16	6.73%	0.946
OSB1:1	31.25	0.27	0.952	0.14	122.02 ± 6.69	5.48%	0.961
OSB2:1	35.17	0.23	0.790	0.14	121.13 ± 6.03	4.98%	0.966
OSB3:1	19.93	0.38	0.910	0.05	151.37 ± 15.11	9.98%	0.932
OSB4:1	23.46	0.33	0.762	0.05	141.83 ± 16.16	11.39%	0.898
OSB5:1	18.43	0.31	0.884	0.03	114.65 ± 11.02	9.61%	0.920

Table 4
Adsorption capacities of phosphate onto OSB3:1 compared with other materials

Material	Pyrolysis temperature	Q_{\max} (mg/g)	References
MgCl ₂ modified banana straw biochar	430°C	31.15	[25]
Nano-rod Ca-decorated sludge derived carbon	800°C	116.82	[26]
Mg/Ca modified biochars	700°C	129.79	[27]
Eggshell modified sludge biochar	800°C	154.18	[28]
La(OH) ₃ modified biochars	400°C	75.08	[10]
Magnetic porous biochar supported La(OH) ₃	180°C	116.08	[29]
Ca(OH) ₂ modified biochar	100°C	138.7	[30]
Calcium aluminate decahydrate	1400°C	89.58	[31]
Sepiolite	900°C	33.9	[32]
Fe/Ca-modified biochar	900°C	33.2	[33]
Eggshell and peanut shells	550°C	130.57	[34]
Potato peels and eggshells	700°C	174.8	[35]
Wheat straw and oyster shells	800°C	151.37	This work

The values of ΔH° and ΔS° were determined by the Van't Hoff equation, and ΔG° was determined by both ΔH° and ΔS° [38]. As shown in Table 5, ΔG° was negative, which suggested that adsorption of phosphate by the modified biochar was a spontaneous process. ΔH° was positive, which indicated that the adsorption was endothermic and phosphate adsorption capacity enhanced with temperature increased (Fig. 7). ΔS° was positive for positive values, which indicated that phosphate had a high extent of freedom at the solid/liquid interface during the adsorption process.

3.2.5. Effect of coexisting anions

SO_4^{2-} , NO_3^- , HCO_3^- , and Cl^- are common anions that coexist with phosphate in aqueous environment. They may impair the phosphate sorption efficiency by increasing the Coulomb repulsion or by binding to the valid reactive sites on the sorbent screen. It showed that NO_3^- , Cl^- , and SO_4^{2-} had negligible effect on the adsorption of phosphate to OSB3:1 (over 95% of removal efficiency), even when the concentration reached to 40 mmol/L. While, HCO_3^- had a relatively obvious impact on the efficiency of phosphate adsorption. As shown in Fig. 8, the adsorption capacity decreased from 64.50 to 58.33 mg/g as the HCO_3^- concentration increases from 0 to 40 mmol/L. The pH of the mixture increased to about 10.5 after adding biochar into phosphorus solution, which can convert HCO_3^- to CO_3^{2-} , and subsequently CO_3^{2-} combined with Ca^{2+} on the surface of OSB3:1 to form CaCO_3 . This process occupied the active sites on the surface of biochar and affected the

generation of Ca-P precipitation, thus reducing the adsorption capacity of biochar. Overall, the decrease of adsorption capacity was not pronounced, which indicated that there was some tolerance of this material for common salts.

3.3. Adsorption mechanism

To reveal the removal mechanism of phosphate by OSB3:1, FTIR, XRD and SEM-EDS analysis of the materials before and after phosphate adsorption were conducted. As seen from the SEM images in Figs. 1 and 9, the obvious difference between the surface of raw OSB3:1 and that after phosphate adsorption happened, suggesting that new substances could be formed on the P-laden OSB3:1 [28]. According to EDS analysis (Fig. 9), the P content of OSB3:1 was very low (1.4%). While, for post-adsorption of OSB3:1, it increased to 8.5%. This indicated that phosphate was successfully trapped by OSB3:1.

Table 5
Thermodynamic parameters for the adsorption of phosphorus on OSB3:1 material

Adsorbents	ΔH° (kJ/mol)	ΔS° (J/mol·K)	ΔG° (kJ/mol)		
			277 K	298 K	318 K
OSB3:1	6.78	25.20	-0.20	-0.73	-1.06

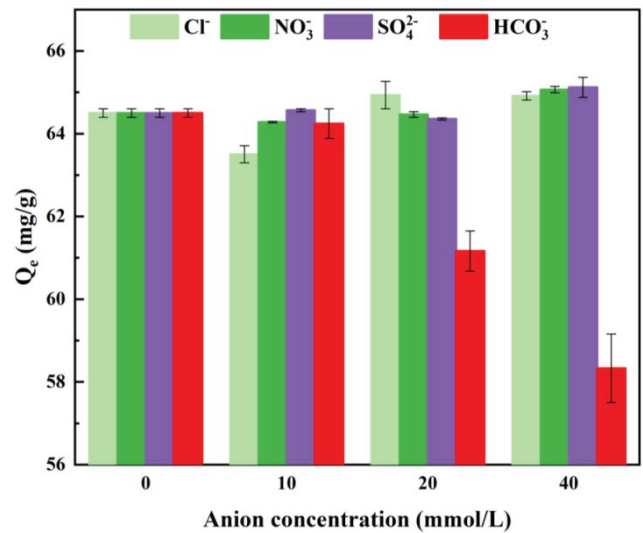


Fig. 8. Effect of co-existing anion on adsorption capacity.

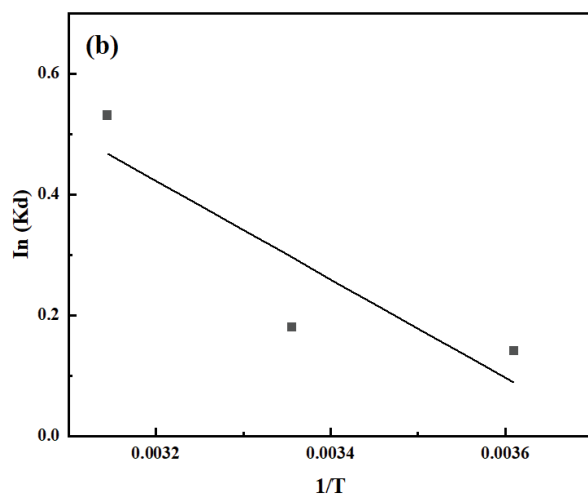
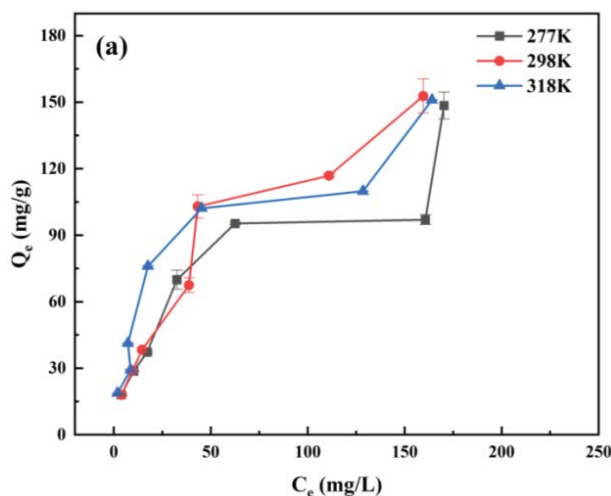


Fig. 7. (a) Adsorption capacity of phosphate on OSB3:1 at different temperatures, and (b) thermodynamic linear fitting.

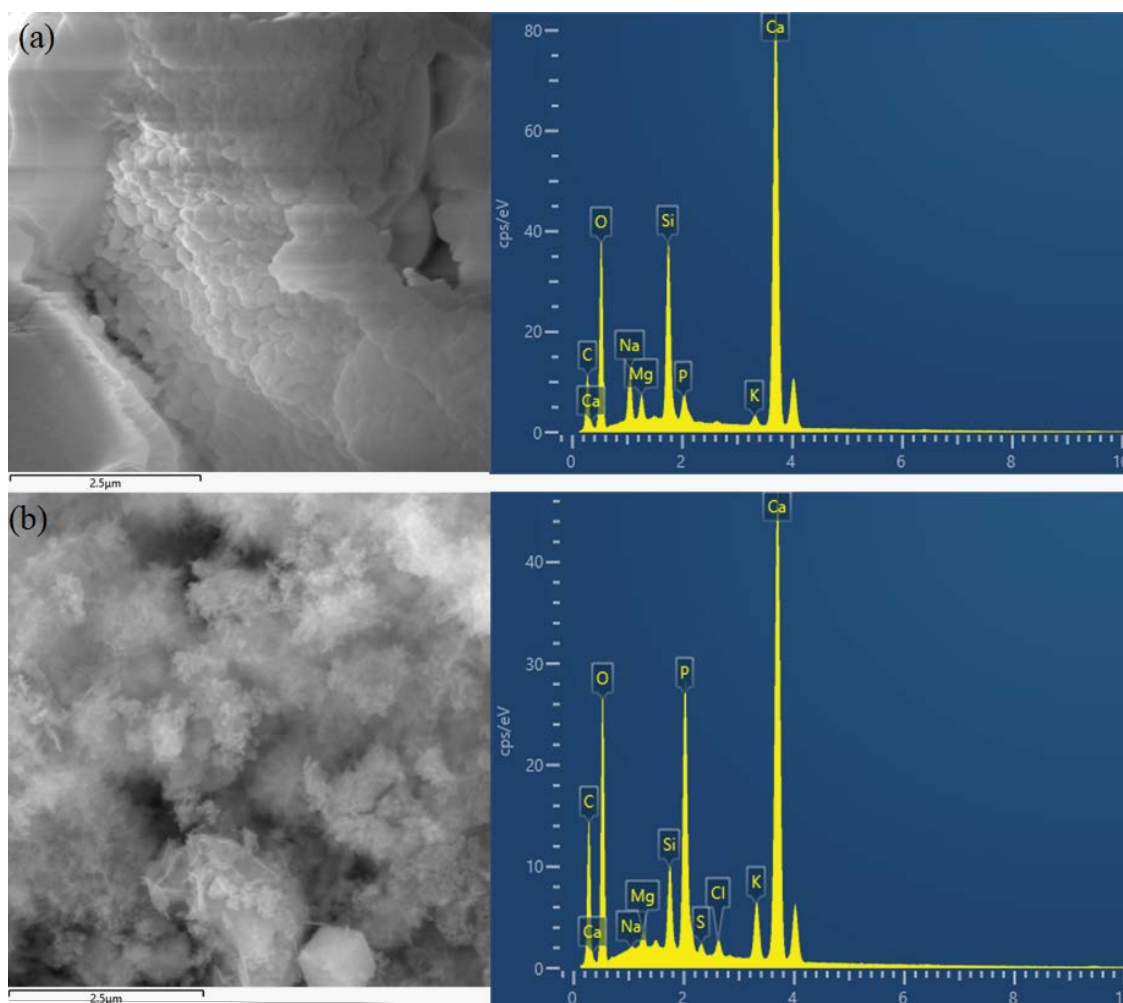


Fig. 9. (a) SEM-EDS images of OSB3:1 and (b) P-laden OSB3:1 after adsorption

XRD analysis was performed for the adsorbents before and after adsorption to investigate the precipitation minerals. After adsorption, the CaO diffraction peaks at $2\theta = 32.5^\circ, 37.8^\circ, 54.2^\circ, 64.7^\circ, 67.7^\circ, 79.9^\circ,$ and 88.8° disappeared, and the diffraction peaks representing Ca(OH)₂ appeared ($2\theta = 18.2^\circ, 34.4^\circ, 47.3^\circ, 51.0^\circ, 54.5^\circ,$ and 54.5°) (Fig. 2). The diffraction peaks representing hydroxyapatite (HAP) (Ca₅(PO₄)₃(OH)) appeared at $28.8^\circ, 29.5^\circ, 32.1^\circ, 39.4^\circ,$ and 49.5° . That indicated that Ca²⁺ reacted with phosphate in the presence of hydroxyl groups to form hydroxyapatite.

FTIR analysis was conducted to further reveal the phosphorus removal mechanism of OSB3:1. For post-adsorption of OSB3:1, a stretching vibration peak belonging to O–P–O appeared at $1,050\text{ cm}^{-1}$ [39], which implies that OSB3:1 successfully adsorbed phosphate from aqueous solution (Fig. 3). After adsorption, the –OH peak at $3,643\text{ cm}^{-1}$ obviously decreased, suggesting that –OH could be involved in the adsorption process (e.g., possible ligand exchange or ion exchange between –OH groups and PO₄³⁻) [13]. Based on the above analysis, the main removal mechanism of phosphate by OSB3:1 included surface precipitation, electrostatic attraction, ligand exchange and ion exchange.

3.4. Ammonium adsorption experiments on modified materials

It is necessary to investigate the ability of OSB3:1 to adsorb ammonium because it is a common pollutant in natural soil and water. In this experiment, the effect of pH on the adsorption of ammonium by OSB3:1 and the isothermal characteristics of the adsorption process were investigated.

As shown in Fig. 10a, ammonium could be adsorbed by OSB3:1 at wide range of pH. Among them, OSB3:1 had the highest adsorption capacity at pH 5 with the Q_c of 0.45 mg/g. The Langmuir and Freundlich models were used to further investigate the adsorption effect of OSB3:1 on ammonium. The fitting results are shown in Fig. 10b and the corresponding parameters are summarized in Table 6. The determined coefficient of the Langmuir isotherm (0.958) was larger than that of the Freundlich (0.927), indicating that the adsorption process could be better described by the Langmuir model. According to the Langmuir model, the maximum adsorption capacity of OSB3:1 for ammonium is 0.80 mg-N/g. From the above experimental results, it concluded that OSB3:1 had a certain adsorption capacity for ammonium, which is beneficial for its application in actual wastewater treatment [40].

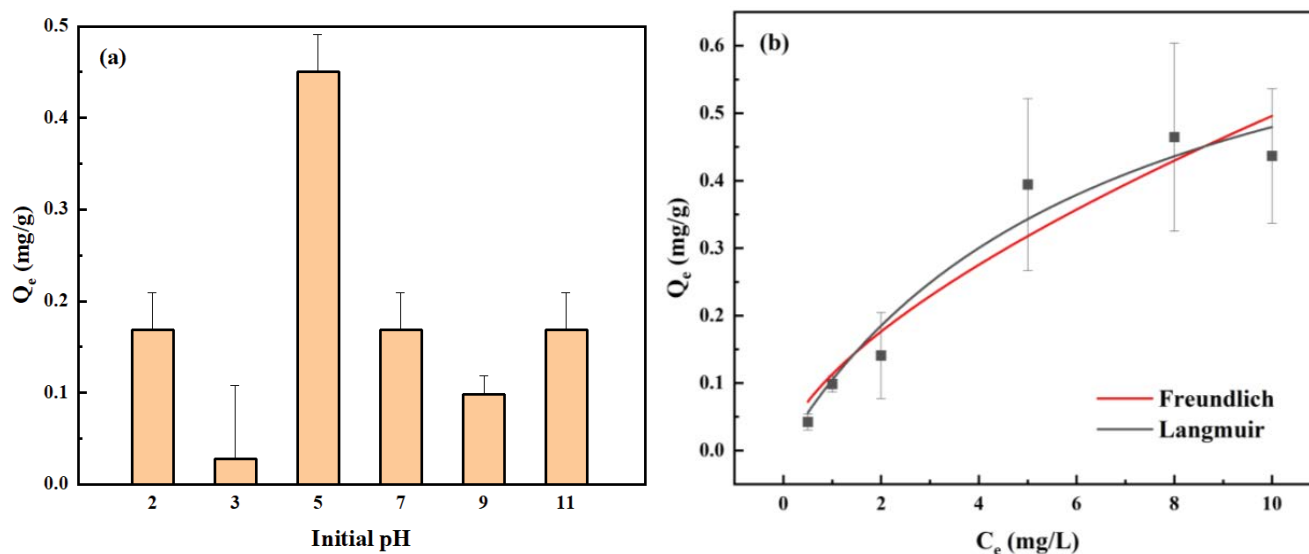


Fig. 10. (a) Effect of initial pH on adsorption capacity of ammonium onto OSB3:1, and (b) adsorption isotherms for ammonium onto OSB3:1.

Table 6
Fitting parameters of ammonium adsorption isotherms on synthetic materials

Absorbents	Freundlich			Langmuir		
	$K_F ((\text{mg/g})(\text{L/mg})^{1/n})$	$1/n$	R^2	$K_L (\text{L/mg})$	$Q_{\text{max}} (\text{mg/g})$	R^2
OSB3:1	0.113	0.643	0.927	0.151	0.80 ± 0.20	0.958

3.5. Potential application for phosphate and ammonium removal

It is necessary to evaluate the adsorption of low concentrations of phosphate onto OSB3:1, due to even phosphate at very low concentration (20 $\mu\text{g/L}$) promoting algal massive growth in natural water body. Therefore, untreated domestic sewage and the treated effluent from wastewater treatment plant of Jinan University in Shandong Province were chosen for phosphate removal at three dosages (1.25, 2.5 and 5 g/L). As shown in Fig. 11a, the removal efficiency of phosphate from domestic wastewater was 71.37% at the dosage of 1.25 g/L, and it gradually increased with the increase of adsorbent dosage, and reached 85.02% when the dosage reached 5 g/L. As shown in Fig. 11b, the effluent concentration of P decreased from 2.50 to 0.87 mg/L within 180 min with the adsorbent dosage of 1.25 g/L. When the modified biochar dosage was further increased to 2.5 and 5 g/L, the phosphate concentration reduced to 0.50 and 0.32 mg/L, respectively. These results suggested that OSB3:1 decreased the effluent concentration of phosphate from actual wastewater. However, it is difficult to further decrease phosphate concentration to trace level. The synthesized material would be suitable for the removal of acidic wastewater with high concentration of phosphate.

As shown in Fig. 11c, the effluent concentration of ammonium decreased from 17.35 to 16.53 mg/L (removal

efficiency of 4.7%) within 180 min with the adsorbent dosage of 1.25 g/L. When the modified biochar dosage was further increased to 2.5 and 5 g/L, the ammonium concentration decreased to 16.19 (removal efficiency of 6.7%) and 15.93 mg/L (removal efficiency of 8.2%), respectively. The similar result of ammonium removal from the effluent of domestic wastewater treatment station is also observed in Fig. 11d. These results showed that OSB3:1 had poor performance on ammonium removal from actual domestic wastewater.

3.6. As adsorbent of heavy metal

The removal efficiency of Cu^{2+} , Cd^{2+} and Zn^{2+} from aqueous solutions by P-laden adsorbent is shown in Fig. 12. The removal efficiency of heavy metals increased with the increase of solution pH, finally reaching more than 99%, and the P-laden adsorbent showed excellent removal ability of Cu^{2+} , Cd^{2+} and Zn^{2+} , especially application for acidic wastewater. Usually, biochar can absorb heavy metals due to its abundant functional groups [41]. In addition, the formed Ca-P precipitates (HAP) in biochar could also contribute heavy metal ions removal from aqueous solution [42]. Thus, reuse of waste P-laden biochar as heavy metal adsorbent was proposed, especially application for acidic wastewater containing heavy metals (e.g., Cu^{2+} , Cd^{2+} and Zn^{2+}).

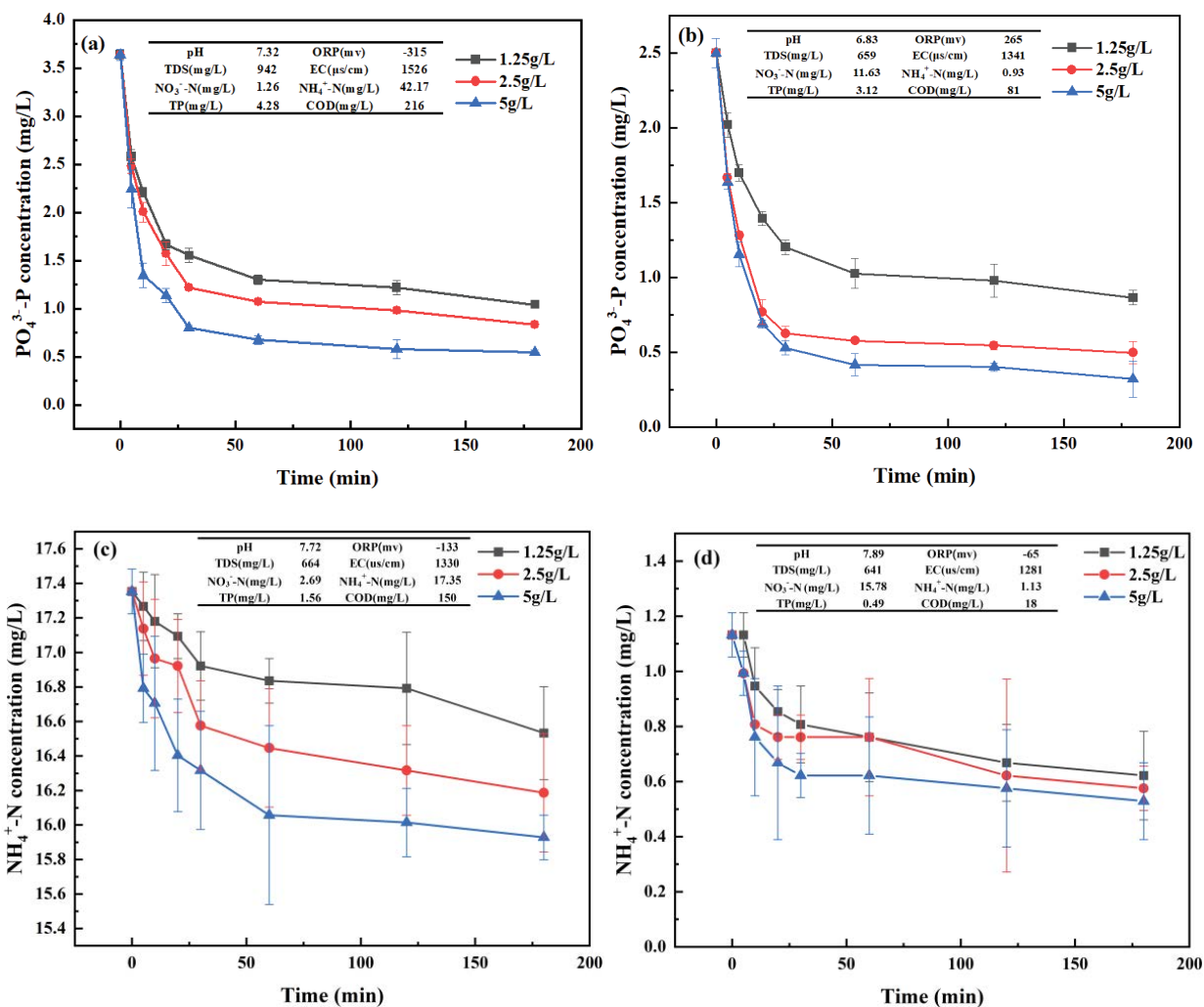


Fig. 11. (a) Phosphate concentration of domestic wastewater treated by OSB3:1, (b) phosphate concentration of effluent from domestic wastewater treatment station treated by OSB3:1, (c) ammonium concentration of domestic wastewater treated by OSB3:1, and (d) ammonium concentration of effluent from domestic wastewater treatment station treated by OSB3:1.

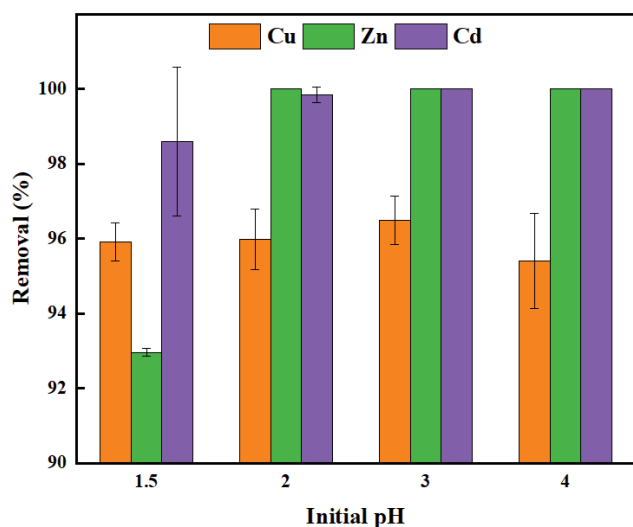


Fig. 12. Removal of heavy metal ions for P-laden OSB3:1

4. Conclusions

In this study, a new calcium-modified biochar was prepared by co-pyrolysis of wheat straw and oyster shell to remove phosphate and ammonium from aqueous solutions. The results showed the biochar composite with the maximum capacity (151.37 mg-P/g and 0.8 mg-N/g) was synthesized at optimum mass ratio (3:1) of oyster shell-to-straw and pyrolysis temperature (800°C). The main adsorption mechanism was the reaction of Ca-loaded biochar with phosphate to form hydroxyapatite, ligand exchange, ion exchange and electrostatic attraction. The synthesized biochar would be suitable for the removal of acidic wastewater with high concentration of phosphate. Reuse of P-laden biochar as heavy metal (e.g., Cd, Zn and Cu) adsorbent was proposed.

Acknowledgement

This study was supported by Shandong Provincial Natural Science Foundation, China (ZR2020ME255), National Key Research and Development Program of China (2017YFD0800601).

References

- [1] X. Liu, L. Zhang, Removal of phosphate anions using the modified chitosan beads: adsorption kinetic, isotherm and mechanism studies, *Powder Technol.*, 277 (2015) 112–119.
- [2] J. Xue, H. Wang, P. Li, M. Zhang, J. Yang, Q. Lv, Efficient reclaiming phosphate from aqueous solution using waste limestone modified sludge biochar: mechanism and application as soil amendments, *Sci. Total Environ.*, 799 (2021) 149454, doi: 10.1016/j.scitotenv.2021.149454.
- [3] J. Cooper, R. Lombardi, D. Boardman, C. Carliell-Marquet, The future distribution and production of global phosphate rock reserves, *Resour. Conserv. Recycl.*, 57 (2011) 78–86.
- [4] Y.V. Nancharaiyah, S.V. Mohan, P.N.L. Lens, Recent advances in nutrient removal and recovery in biological and bioelectrochemical systems, *Bioresour. Technol.*, 215 (2016) 173–185.
- [5] T.H. Pham, K.M. Lee, M.S. Kim, J. Seo, C. Lee, La-modified ZSM-5 zeolite beads for enhancement in removal and recovery of phosphate, *Microporous Mesoporous Mater.*, 279 (2019) 37–44.
- [6] D.D. Nguyen, H.H. Ngo, W. Guo, T.T. Nguyen, S.W. Chang, A. Jang, Y.S. Yoon, Can electrocoagulation process be an appropriate technology for phosphorus removal from municipal wastewater?, *Sci. Total Environ.*, 563 (2016) 549–556.
- [7] Y. Yamazaki, T. Gettongsong, M. Mikawa, Y. Amano, M. Machida, Adsorptive removal of phosphate from water by ammonia gas activated polyacrylonitrile fiber, *J. Fiber Sci. Technol.*, 72 (2016) 237–243.
- [8] D. Yadav, M. Kapur, P. Kumar, M.K. Mondal, Adsorptive removal of phosphate from aqueous solution using rice husk and fruit juice residue, *Process. Saf. Environ.*, 94 (2015) 402–409.
- [9] C. Sun, H. Cao, C. Huang, P. Wang, J. Yin, H. Liu, H. Tian, H. Xu, J. Zhu, Z. Liu, Eggshell based biochar for highly efficient adsorption and recovery of phosphorus from aqueous solution: kinetics, mechanism and potential as phosphorus fertilizer, *Bioresour. Technol.*, 362 (2022) 127851, doi: 10.1016/j.biortech.2022.127851.
- [10] Y. Luo, K. Xie, Y. Feng, Q. He, K. Zhang, S. Shen, F. Wang, Synthesis of a La(OH)₃ nanorod/walnut shell biochar composite for reclaiming phosphate from aqueous solutions, *Colloids Surf., A*, 610 (2021) 125736, doi: 10.1016/j.colsurfa.2020.125736.
- [11] H. Shin, D. Tiwari, D.-J. Kim, Phosphate adsorption/desorption kinetics and P bioavailability of Mg-biochar from ground coffee waste, *J. Water Process Eng.*, 37 (2020) 101484, doi: 10.1016/j.jwpe.2020.101484.
- [12] N. Lv, X. Li, X. Qi, Y. Ren, Calcium-modified granular attapulgite removed phosphorus from synthetic wastewater containing low-strength phosphorus, *Chemosphere*, 296 (2022) 133898, doi: 10.1016/j.chemosphere.2022.133898.
- [13] S. Wang, L. Kong, J. Long, M. Su, Z. Diao, X. Chang, D. Chen, G. Song, K. Shih, Adsorption of phosphorus by calcium-flour biochar: isotherm, kinetic and transformation studies, *Chemosphere*, 195 (2018) 666–672.
- [14] A. Syuhada, M. Ameen, M.T. Azizan, A. Aqsha, M.H.M. Yusoff, A. Ramli, M.S. Alnarabiji, F. Sher, *In-situ* hydrogenolysis of glycerol using hydrogen produced via aqueous phase reforming of glycerol over sonochemically synthesized nickel-based nano-catalyst, *Mol. Catal.*, 514 (2021) 111860, doi: 10.1016/j.mcat.2021.111860.
- [15] Q. Bai, Q. Xiong, C. Li, Y. Shen, H. Uyama, Hierarchical porous cellulose/activated carbon composite monolith for efficient adsorption of dyes, *Cellulose*, 24 (2017) 4275–4289.
- [16] J. Cho, D. Kwon, I. Yang, S. An, J.C. Jung, Unexpected activity of MgO catalysts in oxidative coupling of methane: effects of Ca-promoter, *Mol. Catal.*, 510 (2021) 111677, doi: 10.1016/j.mcat.2021.111677.
- [17] X. Tang, H. Wang, M. Hou, L. Song, C. Zhou, H. Zhao, L. Shi, Highly efficient adsorption of cadmium(II) onto durable coconut fiber residue, *Desal. Water Treat.*, 57 (2016) 15098–15107.
- [18] M.A. Fulazzaky, Z. Majidnia, A. Idris, Mass transfer kinetics of Cd(II) ions adsorption by titania polyvinylalcohol-alginate beads from aqueous solution, *Chem. Eng. J.*, 308 (2017) 700–709.
- [19] M.A. Fulazzaky, Determining the resistance of mass transfer for adsorption of the surfactants onto granular activated carbons from hydrodynamic column, *Chem. Eng. J.*, 166 (2011) 832–840.
- [20] Y. Peng, D. Xiao, G. Yu, Y. Feng, J. Li, X. Zhao, Y. Tang, L. Wang, Q. Zhang, Effect of an eco-friendly o/w emulsion stabilized with amphiphilic sodium alginate derivatives on lambda-cyhalothrin adsorption-desorption on natural soil minerals, *J. Environ. Sci.*, 78 (2019) 230–238.
- [21] Q. Feng, M. Chen, P. Wu, X. Zhang, S. Wang, Z. Yu, B. Wang, Simultaneous reclaiming phosphate and ammonium from aqueous solutions by calcium alginate-biochar composite: sorption performance and governing mechanisms, *Chem. Eng. J.*, 429 (2022) 132166, doi: 10.1016/j.cej.2021.132166.
- [22] M.A. Fulazzaky, Analysis of global and sequential mass transfers for the adsorption of atrazine and simazine onto granular activated carbons from a hydrodynamic column, *Anal. Methods*, 4 (2012) 2396–2403.
- [23] Y. Zhou, Y. Li, X. Wang, D. Liu, D. Liu, Preparation of amidoxime functionalized titanate nanosheets for efficient extraction of uranium from aqueous solution, *J. Solid State Chem.*, 290 (2020) 121562, doi: 10.1016/j.jssc.2020.121562.
- [24] Y. Feng, Y. Luo, Q. He, D. Zhao, K. Zhang, S. Shen, F. Wang, Performance and mechanism of a biochar-based Ca-La composite for the adsorption of phosphate from water, *J. Environ. Chem. Eng.*, 9 (2021) 105267, doi: 10.1016/j.jece.2021.105267.
- [25] Y.H. Jiang, A.Y. Li, H. Deng, C.H. Ye, Y.Q. Wu, Y.D. Linmu, H.L. Hang, Characteristics of nitrogen and phosphorus adsorption by Mg-loaded biochar from different feedstocks, *Bioresour. Technol.*, 276 (2019) 183–189.
- [26] L. Kong, M. Han, K. Shih, M. Su, Z. Diao, J. Long, D. Chen, L. Hou, Y. Peng, Nano-rod Ca-decorated sludge derived carbon for removal of phosphorus, *Environ. Pollut.*, 233 (2018) 698–705.
- [27] L. Fang, J.-s. Li, S. Donatello, C.R. Cheeseman, C.S. Poon, D.C.W. Tsang, Use of Mg/Ca modified biochars to take up phosphorus from acid-extract of incinerated sewage sludge ash (ISSA) for fertilizer application, *J. Cleaner Prod.*, 244 (2020) 118853, doi: 10.1016/j.jclepro.2019.118853.
- [28] J. Li, L. Cao, B. Li, H. Huang, W. Yu, C. Sun, K. Long, B. Young, Utilization of activated sludge and shell wastes for the preparation of Ca-loaded biochar for phosphate removal and recovery, *J. Cleaner Prod.*, 382 (2023) 135395, doi: 10.1016/j.jclepro.2022.135395.
- [29] Y. Zhang, M.S. Akindolie, X. Tian, B. Wu, Q. Hu, Z. Jiang, L. Wang, Y. Tao, B. Cao, J. Qu, Enhanced phosphate scavenging with effective recovery by magnetic porous biochar supported La(OH)₃: kinetics, isotherms, mechanisms and applications for water and real wastewater, *Bioresour. Technol.*, 319 (2021) 124232, doi: 10.1016/j.biortech.2020.124232.
- [30] S. Zeng, E. Kan, Sustainable use of Ca(OH)₂ modified biochar for phosphorus recovery and tetracycline removal from water, *Sci. Total Environ.*, 839 (2022) 156159, doi: 10.1016/j.scitotenv.2022.156159.
- [31] P. Cheng, Y. Liu, L. Yang, Q. Ren, X. Wang, Y. Chi, H. Yuan, S. Wang, Y.-X. Ren, Phosphate adsorption using calcium aluminate decahydrate to achieve low phosphate concentrations: batch and fixed-bed column studies, *J. Environ. Chem. Eng.*, 11 (2023) 109377, doi: 10.1016/j.jece.2023.109377.
- [32] H. Yin, M. Kong, C. Fan, Batch investigations on P immobilization from wastewaters and sediment using natural calcium rich sepiolite as a reactive material, *Water Res.*, 47 (2013) 4247–4258.
- [33] W. Ou, X. Lan, J. Guo, A. Cai, P. Liu, N. Liu, Y. Liu, Y. Lei, Preparation of iron/calcium-modified biochar for phosphate removal from industrial wastewater, *J. Cleaner Prod.*, 383 (2023) 135468, doi: 10.1016/j.jclepro.2022.135468.
- [34] X. Liu, J. Lv, Efficient phosphate removal from wastewater by Ca-laden biochar composites prepared from eggshell and peanut shells: a comparison of methods, *Sustainability*, 15 (2023) 1778, doi: 10.3390/su15031778.

- [35] A. Quisperima, S. Pérez, E. Flórez, N. Acelas, Valorization of potato peels and eggshells wastes: Ca-biocomposite to remove and recover phosphorus from domestic wastewater, *Bioresour. Technol.*, 343 (2022) 126106, doi: 10.1016/j.biortech.2021.126106.
- [36] D. Suteu, S. Coseri, M. Badeanu, C. Zaharia, Valorization of food wastes as sorbent for dye retention from aqueous medium, *Desal. Water Treat.*, 54 (2015) 2570–2580.
- [37] I.K. Rind, A. Sari, M. Tuzen, M.F. Lanjwani, I. Karaman, T.A. Saleh, Synthesis of bentonite/SiO₂/magnetite nanostructure as an efficient adsorbent for Bisphenol A removal from waters, *Ind. Crops Prod.*, 201 (2023) 116905, doi: 10.1016/j.indcrop.2023.116905.
- [38] A.P. Panda, P. Rout, S.A. Kumar, U. Jha, S.K. Swain, Enhanced performance of a core-shell structured Fe(0)@Fe oxide and Mn(0)@Mn oxide (ZVIM) nanocomposite towards remediation of arsenic contaminated drinking water, *J. Mater. Chem. A*, 8 (2020) 4318–4333.
- [39] X. Liu, J. Fu, Y. Tang, R.L. Smith Jr., X. Qi, Mg-coordinated self-assembly of MgO-doped ordered mesoporous carbons for selective recovery of phosphorus from aqueous solutions, *Chem. Eng. J.*, 406 (2021) 126748, doi: 10.1016/j.cej.2020.126748.
- [40] G. Fu, Y. Zhao, S. Zhou, C. Chen, Y. Zhong, Y. Xu, Efficient removal of nitrogen and phosphorus in aqueous solutions using modified water treatment residuals–sodium alginate beads, *Environ. Sci. Pollut. Res.*, 28 (2021) 46233–46246.
- [41] I.K. Rind, A. Sari, M. Tuzen, M.F. Lanjwani, I. Karaman, T.A. Saleh, Influential biosorption of lead from aquatic solution using *Escherichia coli*/carbon nanofibers, *Environ. Nanotechnol. Monit. Manage.*, 19 (2023) 100776, doi: 10.1016/j.enmm.2022.100776.
- [42] L. Pei, F. Yang, X. Xu, H. Nan, X. Gui, L. Zhao, X. Cao, Further reuse of phosphorus-laden biochar for lead sorption from aqueous solution: isotherm, kinetics, and mechanism, *Sci. Total Environ.*, 792 (2021) 148550, doi: 10.1016/j.scitotenv.2021.148550.